Please cite this article in press as: Jokhi et al., Torsin Mediates Primary Envelopment of Large Ribonucleoprotein Granules at the Nuclear Envelope, Cell Reports (2013), http://dx.doi.org/10.1016/j.celrep.2013.03.015

Cell Reports
Report

Cell PRESS
Open ACCESS

Torsin Mediates Primary Envelopment of Large Ribonucleoprotein Granules at the Nuclear Envelope

Vahbiz Jokhi,[1,4] James Ashley,[1,4] John Nunnari,[1] Akiko Noma,[2] Naoto Ito,[3] Noriko Wakabayashi-Ito,[3] Melissa J. Moore,[2] and Vivian Budnik[1,*]
[1]Department of Neurobiology
[2]RNA and Neuro Therapeutics Institutes, Department of Biochemistry and Molecular Pharmacology, Howard Hughes Medical Institute University of Massachusetts Medical School, Worcester, MA 01605, USA
[3]Department of Neurology and Radiology, Massachusetts General Hospital and Program in Neuroscience, Harvard Medical School, Boston, MA 02114, USA
[4]These authors contributed equally to this work
*Correspondence: vivian.budnik@umassmed.edu
http://dx.doi.org/10.1016/j.celrep.2013.03.015

SUMMARY

A previously unrecognized mechanism through which large ribonucleoprotein (megaRNP) granules exit the nucleus is by budding through the nuclear envelope (NE). This mechanism is akin to the nuclear egress of herpes-type viruses and is essential for proper synapse development. However, the molecular machinery required to remodel the NE during this process is unknown. Here, we identify Torsin, an AAA-ATPase that in humans is linked to dystonia, as a major mediator of primary megaRNP envelopment during NE budding. In *torsin* mutants, megaRNPs accumulate within the perinuclear space, and the messenger RNAs contained within fail to reach synaptic sites, preventing normal synaptic protein synthesis and thus proper synaptic bouton development. These studies begin to establish the cellular machinery underlying the exit of megaRNPs via budding, offer an explanation for the "nuclear blebbing" phenotype found in dystonia models, and provide an important link between Torsin and the synaptic phenotypes observed in dystonia.

INTRODUCTION

Polarized assembly of cellular complexes often depends on formation of translationally silent RNA transport granules containing mRNAs and associated structural and regulatory components (e.g., proteins and microRNAs). These RNA-protein complexes (RNPs) are shuttled to distinct cellular locales where, upon specific stimuli, the messenger RNAs (mRNAs) are translated into protein building blocks for local cellular architectures and macromolecular complexes (Richter, 2001). Particularly notable is RNP transport in the nervous system, where long-term changes in synaptic structure and function frame key events enabling organisms to respond to their changing environment. A special case of this adaptation is the ability of organisms to learn and remember (Wiersma-Meems et al., 2005). In these processes, localized translation of mRNAs links synaptic-plasticity-inducing stimuli to the synthesis of effector proteins underlying enduring changes in synaptic structure and function (Barco et al., 2008).

Until recently, it was thought that all mRNA export occurred one molecule at a time through the nuclear pore complex (NPC) (Grünwald et al., 2011; Köhler and Hurt, 2007). However, we recently uncovered a mechanism by which large ribonucleoprotein (megaRNP) granules exit the nucleus via nuclear envelope (NE) budding (Speese et al., 2012), a mechanism previously shown to be utilized for the nuclear export of large herpes-type viral capsids (Maric et al., 2011; Mettenleiter et al., 2006). This budding process and the signaling pathway that it initiates are essential for normal synaptic bouton development at the *Drosophila* larval neuromuscular junction (NMJ) (Ataman et al., 2006; Mathew et al., 2005; Speese et al., 2012). NE budding entails primary envelopment of viral capsids (Mettenleiter et al., 2006) or megaRNPs (Speese et al., 2012) by the inner nuclear membrane (INM); scission of this envelope from the INM creates a membrane-bound particle within the perinuclear space, which subsequently fuses with the outer nuclear membrane (ONM) to allow nuclear escape of the enclosed material. However, the molecular mechanisms required for primary envelopment, INM scission, and fusion were previously unknown. Here, we identify Torsin, an AAA-ATPase that in humans is linked to both dystonia (Breakefield et al., 2008) and herpes virus nuclear egress (Maric et al., 2011), as a major mediator of primary megaRNP envelopment during NE budding, likely functioning to promote INM scission. In *torsin* mutants, including those mimicking genetic abnormalities in dystonia patients, megaRNPs accumulate within the perinuclear space and the mRNAs contained within fail to reach synaptic sites, preventing normal synaptic protein synthesis and thus proper synaptic bouton development.

RESULTS AND DISCUSSION

In humans, the dystonia-specific *Torsin1A* (*TOR1A*) mutation $TOR1A^{\Delta E302/303}$ (also known as $TOR1A^{\Delta GAG}$; referred to as $Torsin^{\Delta E}$ in this paper) at the DYT1 gene locus is linked to

Please cite this article in press as: Jokhi et al., Torsin Mediates Primary Envelopment of Large Ribonucleoprotein Granules at the Nuclear Envelope, Cell Reports (2013), http://dx.doi.org/10.1016/j.celrep.2013.03.015

Cell PRESS
Open ACCESS

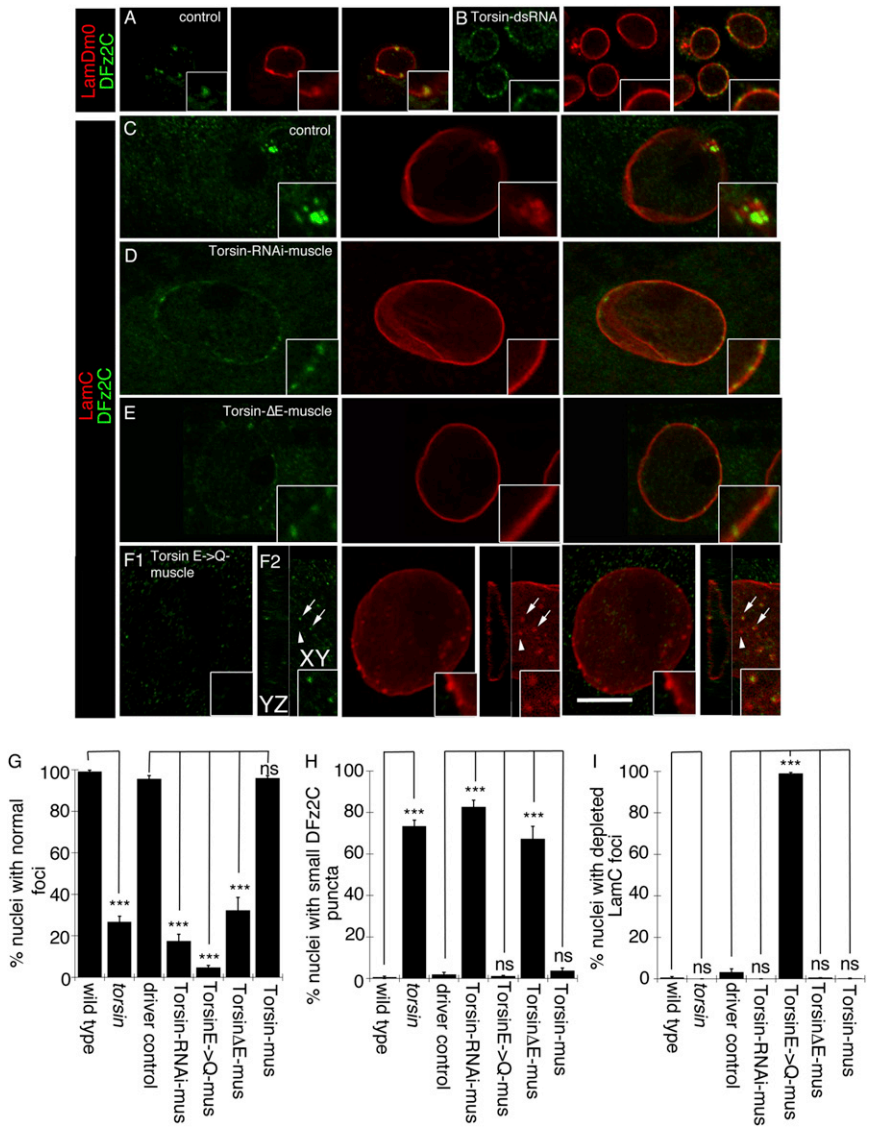

Figure 1. Morphology of Nuclear DFz2C/Lam Foci Is Disrupted in Torsin Mutations

(A and B) Localization and morphology of DFz2C/Lam foci at the nuclei of S2 cells in (A) untreated cells and (B) cells treated with Torsin-dsRNA.

(C–F) Localization and morphology of nuclear DFz2C/LamC foci in larval muscles of (C) wild-type and (D–F) larvae expressing (D) Torsin RNAi, (E) Torsin$^{\Delta E}$, and (F) Torsin$^{E\rightarrow Q}$ in muscles. F1 is a low-magnification view. F2 shows a high-magnification view of DFz2 puncta in the YZ and XY planes. (A)–(F) correspond to singe confocal slices.

(G–I) Percentage of nuclear foci showing (G) normal organization of DFz2C/LamC, (H) the presence of small DFz2C puncta associated with the lamina (see text), and (I) the presence of thickenings of the lamina devoid of DFz2C signal. Mus, muscle; N([number of nuclei;number of larvae]), [908;6],[731;6],[639;6],[802;6],[846;6],[733;6],[693;6]. Error bars represent ±SEM; ***$p < 0.0001$.

Calibration scales are 14 μm (4 μm for insets) in (A) and (B) and 10 μm (6 μm for insets) in (C)–(F). See also Figure S1.

Figure S1 for Torsin-dsRNA efficiency). This resulted in significant abnormalities in DFz2C/LamC foci at the NE. In untreated S2 cells, NE-DFz2C foci appear as bright immunoreactive spots embedded in a thickening of the lamina, marked by LamC (Speese et al., 2012) or the B-type lamin LamDm0 (Figure 1A). In contrast, Torsin-dsRNA-treated cells displayed small DFz2C-immunoreactive puncta dotting the NE, and thickenings of the lamina were barely visible or absent (Figure 1B; see below for quantification of this phenotype in vivo).

In mammals, Torsin isoforms are derived from four genes: *Tor1A*, *Tor1B*, *Tor2A*, and *Tor3A*. The DYT1 mutation in *Tor1A* specifically affects the neuronal NE (Goodchild et al., 2005), consistent with the belief that dystonia is a disease of the nervous system. This neuronal specificity is likely due to compensation by expression of torsinB in nonneuronal tissues, as knockdown of TOR1B in a DYT mutant background caused NE defects in nonneuronal cells (Kim et al., 2010). In *Drosophila*, there is a single *torsin* gene, thus overcoming difficulties associated with redundancy. Moreover, we previously showed that NE budding occurs in several cell types, including larval body wall muscle cells wherein the large nuclei are particularly suitable for high-resolution studies (Speese et al., 2012). In addition, the glutamatergic larval NMJ is a powerful model system in which to understand mechanisms of synapse development and function.

To determine the significance of the S2 cell NE phenotype upon Torsin downregulation, DFz2C/LamC foci were examined in *torsin*^{KO78}-null mutants (Wakabayashi-Ito et al., 2011) and in early-onset primary dystonia (Tanabe et al., 2009). Mouse models expressing *TOR1A*$^{\Delta E302/303}$ accumulate abnormal vesicular structures at the NE (Goodchild et al., 2005; Naismith et al., 2004). These NE structures show a striking resemblance to the perinuclear megaRNPs we recently reported in *Drosophila* (Speese et al., 2012), raising the intriguing possibility that these structures could be related. In cultured Schneider-2 (S2) cells and *Drosophila* larval muscles, megaRNP clusters at the NE can be marked at the light microscopy level by antibodies to the C terminus of the Wnt receptor DFrizzled2 (DFz2C) and the INM-associated protein Lamin C (LamC). DFz2C and LamC partially colocalize at NE-associated foci (DFz2C/LamC foci) (Mathew et al., 2005; Speese et al., 2012). To determine if NE defects observed in *TOR1A* mutant animal models reflect defects in NE budding, S2 cells were treated with Torsin double-stranded RNA (dsRNA), targeting the sole *Drosophila* homolog of mammalian *TOR1A* (Wakabayashi-Ito et al., 2011) (see

larvae in which Torsin was specifically downregulated in muscles by expressing Torsin RNAi using the muscle-specific Gal4 driver C57-Gal4 (Budnik et al., 1996). As in untreated S2 cells, NE DFz2C/LamC foci were observed in wild-type larvae as DFz2C immunoreactive spots surrounded by a thickening of LamC immunoreactivity (Speese et al., 2012) (Figure 1C). In contrast, in larvae expressing Torsin-RNAi in muscles (Figure 1D) or in *torsin*-null mutants, DFz2C foci were observed as small puncta decorating the NE but lacking any detectable thickening of the lamina. These phenotypes were quantified by determining the percentage of nuclei containing DFz2C spots surrounded by a thickening of the lamina (normal foci; Figure 1G) and the percentage of nuclei containing small NE-associated DFz2C puncta lacking LamC thickening (Figure 1H). There were highly significant differences between wild-type controls and both *torsin*-null mutants as well as larvae expressing Torsin-RNAi in muscles (Figures 1G and 1H).

Typical of AAA-ATPases, Torsin contains Walker A and Walker B domains involved in ATP binding and ATP hydrolysis, respectively (Neuwald et al., 1999; Wakabayashi-Ito et al., 2011; Walker et al., 1982), as well as Sensor1 and Sensor2 domains also involved in ATP hydrolysis (Iyer et al., 2004). A conserved amino acid deletion in the Sensor2 domain (Torsin$^{\Delta E}$; Torsin$^{\Delta E306}$ in *Drosophila*) is dominantly linked to dystonia (Ozelius et al., 1997). In addition, an amino acid substitution in the Walker B domain (Torsin$^{E\rightarrow Q}$; Torsin^{E177Q} in *Drosophila*) leads to a Torsin protein that can dominantly bind to its substrate but is unable to hydrolyze ATP and therefore remains bound to this substrate, thus constituting a substrate trap (Goodchild et al., 2005; Wakabayashi-Ito et al., 2011). To determine if Torsin$^{\Delta E}$ or Torsin$^{E\rightarrow Q}$ transgene expression would also disrupt DFz2C/LamC foci morphology, we expressed these proteins in larval muscles. Expressing Torsin$^{\Delta E}$ mimicked the *torsin*-null and Torsin-RNAi phenotypes (Figures 1E, 1G, and 1H). In contrast, Torsin$^{E\rightarrow Q}$ expression resulted in the formation of numerous NE LamC foci, most of which were devoid of DFz2C immunoreactivity (Figures 1F1 and 1G–1I). Careful examination of these depleted LamC foci by confocal microscopy demonstrated that many contained a small DFz2C puncta, but this signal was barely visible (Figure 1F2, arrows). The above phenotypes observed upon expressing Torsin$^{\Delta E}$ and Torsin$^{E\rightarrow Q}$ were the specific results of the mutations in the Torsin transgenes, as larvae expressing a wild-type Torsin transgene were indistinguishable from wild-type not expressing this transgene (Figures 1G–1I).

To determine the ultrastructural correlates of the above phenotypes, untreated and Torsin-dsRNA-treated S2 cells were examined by transmission electron microscopy (TEM). As previously described (Speese et al., 2012), untreated S2 cells displayed local singlets or clusters of megaRNPs within INM invaginations at discrete regions of the NE (Figures 2A, 2H, and 2I), paralleling light microscopy observations (Figure 1A). In contrast, in Torsin-dsRNA-treated cells, these local megaRNPs at the NE were reduced by ~75% (Figures 2H and 2I), and instead many mega-RNP granules were often observed in rows of singlets lining the perinuclear space (Figures 2B and 2C). In these regions, the perinuclear space appeared distended (green in Figures 2B and 2C) and the ribosome-decorated ONM appeared to evaginate (Figures 2B and 2C). However, NPCs and the rest of the NE appeared normal (Figures S2A–S2D). In addition, the distribution of a number of nuclear proteins, such as the fly Emerin homolog Bocksbeutel (Figures S2E and S2I); dMan1 (Figures S2F and S2J); Otefin, a protein required for NE assembly (Figures S2G and S2K); and the *Drosophila* homolog of Hsap, Squid, a ribonuclear protein (Figures S2H and S2L), were normally distributed in the mutants. About half of megaRNPs appeared attached to the INM through a collared neck (arrows in Figures 2B, 2C, 2H, and 2I; see Experimental Procedures for definition). Thus, downregulating Torsin results in abnormal attachment of megaRNPs to the INM, raising the possibility that Torsin could be involved in INM scission after primary megaRNP envelopment.

Corroboration of the above results in vivo was obtained by examining larval body wall muscles of *torsin*-null mutants. As in S2 cells, megaRNPs tethered to the INM by a collared neck were observed in *torsin*-null mutant muscles and epithelial cells (Figures 2D, 2E, 2H, and 2I), suggesting this pathway functions in even more tissues than previously characterized. Similarly, muscles expressing Torsin$^{E\rightarrow Q}$ displayed INM-tethered megaRNPs (Figures 2F, 2H, and 2I). In ~30% of cases, megaRNPs in muscles expressing Torsin$^{E\rightarrow Q}$ appeared as large (>250 nm), amorphous, dense structures directly apposed to the INM (Figures 2G–2I). Thus, disruption of Torsin function in vivo leads to abnormal megaRNP tethering to the INM.

If Torsin is involved in INM scission during megaRNP primary envelopment, then the substrate trap Torsin$^{E\rightarrow Q}$ should accumulate at the electron-dense collared necks. This prediction was tested by generating wild-type and Torsin$^{E\rightarrow Q}$ variants fused to a mini-SOG tag (Shu et al., 2011) at their C termini. Mini-SOG is a flavoprotein derived from *Arabidopsis* Phototropin 2 that when illuminated by blue light produces oxygen species that can convert diaminobenzidine into an electron-dense precipitate (Shu et al., 2011).

We first determined if C-terminally tagged Torsin was localized to the NE. Although mini-SOG excitation results in fluorescence emission, its rapid bleaching upon illumination prevented high-resolution acquisition of images. Therefore, we generated Flag-tagged Torsin constructs and expressed them in S2 cells. The wild-type Torsin-Flag signal localized to bright spots coinciding with Lamin foci at the NE; low levels were also observed at the NE and in the cytoplasm (Figure 3A). In contrast, Torsin$^{E\rightarrow Q}$-Flag was observed in a punctate pattern lining the NE (Figure 3B).

Consistent with the above observations, S2 cells expressing Torsin-SOG displayed an electron-dense signal at sites of megaRNP occurrence in the NE (Figures 3C and 3E; see Figures S3A and S3B for specificity control). An electron-dense SOG-induced signal surrounded each megaRNP (Figures 3C and 3E) in a relatively homogenous fashion, but local accumulations of the signal were also apparent (arrows in Figure 3E). A SOG-specific signal was also observed at the INM and ONM in proximity to megaRNPs (Figure 3E). In contrast, in cells expressing the substrate trap Torsin$^{E\rightarrow Q}$-SOG, a SOG-induced signal was concentrated at collared necks of INM-associated megaRNPs and little SOG signal surrounded the megaRNPs (Figures 3D and 3F). In cases where large amorphous megaRNPs were tightly apposed to the INM in Torsin$^{E\rightarrow Q}$, the SOG signal was considerably denser at the sites of contact between the megaRNP and the INM (Figure 3G). These observations suggest

Please cite this article in press as: Jokhi et al., Torsin Mediates Primary Envelopment of Large Ribonucleoprotein Granules at the Nuclear Envelope, Cell Reports (2013), http://dx.doi.org/10.1016/j.celrep.2013.03.015

Cell PRESS
Open ACCESS

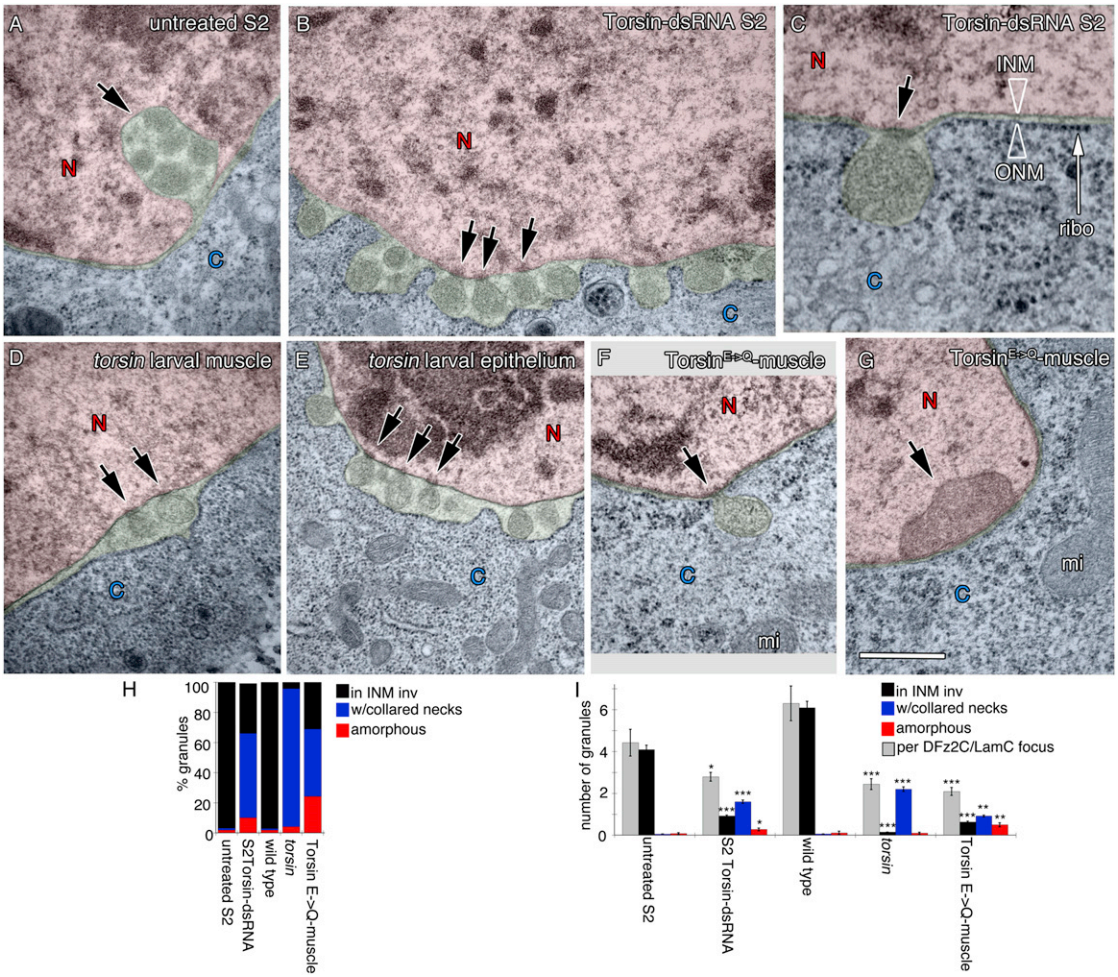

Figure 2. Ultrastructural Organization of NE-Associated megaRNPs Is Disrupted in Torsin Mutations

(A–G) Electron micrographs of nuclear regions in (A–C) S2 cells, (D, F, and G) larval body wall muscles, and (E) larval epithelial cells showing NE-associated megaRNPs. Red, nucleus; blue, cytoplasm; green, perinuclear space. N, nucleus; C, cytoplasm. (A) Untreated S2 cell showing a normal nuclear focus (arrow) containing electron-dense megaRNP granules. (B and C) NE of Torsin-dsRNA-treated S2 cells displaying megaRNPs tethered to the INM by collared necks (arrows), shown at (B) low and (C) high magnification. ribo, ribosome. (D and E) NE in *torsin*-null mutants also showing megaRNPs tethered to the INM (arrows). (F and G) NE in muscle cells expressing Torsin$^{E\rightarrow Q}$ showing the presence of (F) a megaRNP (arrow) tethered to the INM and (G) a large, amorphous megaRNP (arrow) tightly apposed to the INM. mi, mitochondria.

(H) Percentage of megaRNP granules present in INM invaginations (black), with collared necks (blue) and being large and amorphous (red).

(I) Average number of megaRNP granules in INM invaginations (black), with collared necks (blue), being large and amorphous (red), or per focus (gray). N[number of granules;foci]), [159;36],[366;122],[207;33],[166;68],[181;88]. Error bars represent ±SEM; *$p < 0.05$; **$p < 0.001$; ***$p < 0.0001$).

Calibration scales are 0.5 μm (A, B, and D–G) and 0.2 μm (C). See also Figure S2.

that Torsin is present at sites of NE budding. Further, accumulation of the Torsin$^{E\rightarrow Q}$ substrate trap protein at collared necks of megaRNPs suggests that these necks represent the normal site of Torsin action and provide evidence that Torsin is involved in scission of the INM during primary envelopment.

Our previous study revealed that in *Drosophila* larval muscles, megaRNPs contain transcripts encoding postsynaptic proteins, including the PDZ scaffolding proteins Par6 and MAGI (Speese et al., 2012). In the case of Par6, interfering with megaRNP formation by inhibiting the Frizzled nuclear import (FNI) pathway or LamC expression results in decreased NMJ localization of *par6* mRNA (Speese et al., 2012), decreased postsynaptic Par6 protein levels (Speese et al., 2012), and marked defects in NMJ structure (Ataman et al., 2006, 2008; Packard et al., 2002; Speese et al., 2012). In particular, under these conditions, NMJs fail to expand normally as muscles grow in size during larval development, and a subset of synaptic boutons (called ghost boutons) remain in an immature state. These ghost boutons fail to recruit postsynaptic proteins and to organize postsynaptic specializations, such as the postsynaptic density and subsynaptic reticulum (Ataman et al., 2006, 2008; Packard et al., 2002; Speese et al., 2012).

The above observations support a model in which alterations in Torsin function inhibit nuclear megaRNP exit by slowing or

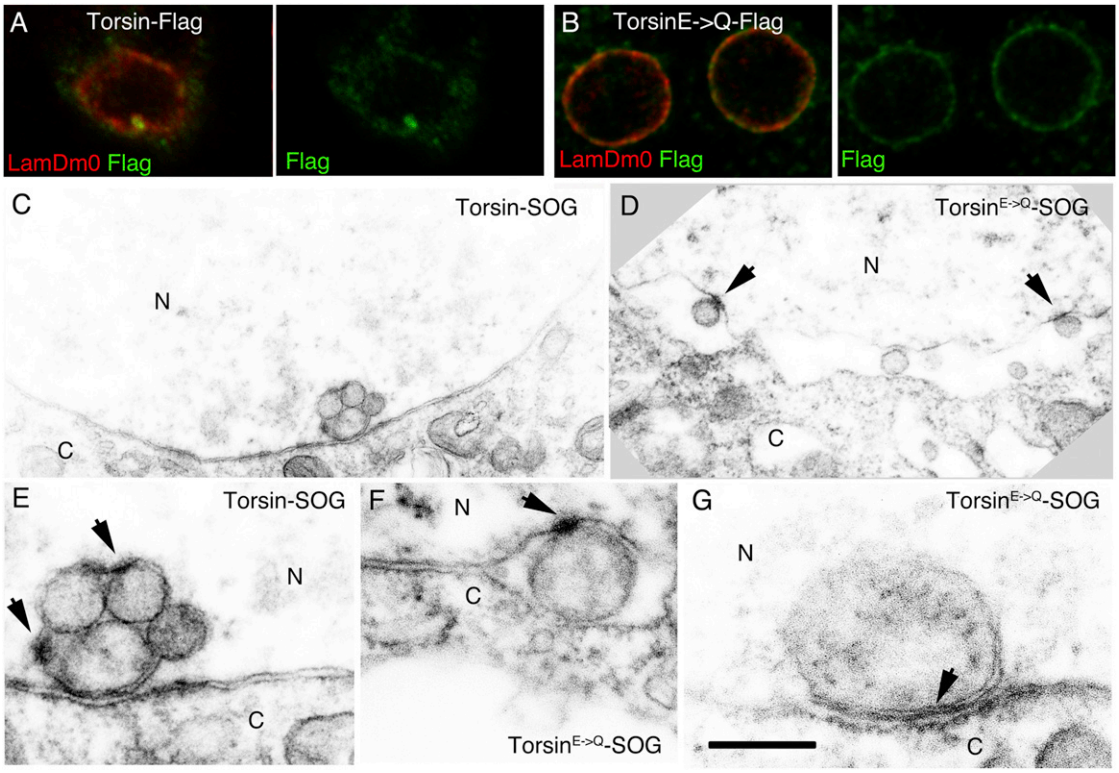

Figure 3. The Torsin$^{E\rightarrow Q}$ Protein Accumulates at megaRNP Collared Necks

(A and B) S2 cells expressing (A) wild-type Torsin-Flag and (B) the Torsin$^{E\rightarrow Q}$-Flag showing that Torsin-Flag accumulates at foci and Torsin$^{E\rightarrow Q}$ is punctate at the NE.

(C–G) Electron micrographs of nuclear regions of S2 cells expressing (C and E) Torsin-SOG showing an electron-dense signal surrounding megaRNPs (arrows point to areas of increased signal density). (D, F, and G) Torsin$^{E\rightarrow Q}$-SOG showing that signal accumulates (D and F) at megaRNP collared necks or (G) at appositions of amorphous megaRNPs with the INM.

Calibration scales are 7 μm (A and B), 0.7 μm (C and D), and 0.3 μm (E–G). See also Figure S3.

blocking INM scission during primary envelopment. As a consequence, such alterations should result in abnormal transcript localization both in the nucleus and at synaptic sites as well as decreased synaptic protein synthesis, abnormal NMJ expansion, and an accumulation of ghost boutons. To ascertain the localization of megaRNP transcripts known to be present in megaRNPs at the NE, we carried out fluorescence in situ hybridization (FISH) using *par6* and *magi* RNA probes. As previously described (Speese et al., 2012), in wild-type muscles, *par6* and *magi* mRNAs are enriched at NE foci associated with LamC foci or nuclear folds marked by antibodies to LamC (Figures 4A and 4B, top row). In contrast, in *torsin*-null mutants, *par6* and *magi* FISH signals appeared as foci that, while associated with the NE, were on the cytoplasmic side of the LamC signal (Figures 4A and 4B, bottom row panels; Figure 4C). This is in agreement with the light and electron microscopy studies, showing that altering Torsin function prevents megaRNP nuclear egress and results in megaRNPs remaining attached to the INM within the perinuclear space.

When we examined FISH signals at the NMJ in wild-type controls, *par6* mRNA was concentrated at subsynaptic sites as previously reported (Figure 4D, top panels) (Speese et al., 2012). However, this synaptic *par6* FISH signal was virtually eliminated in *torsin*-null mutants (Figure 4D, bottom panels). Similarly, the synaptic localization of *magi* mRNA was significantly decreased in the *torsin* mutants (Figure 4E). The marked decrease in *par6* and *magi* mRNA levels at the NMJ appeared specific for the NE-budding pathway, as no significant differences around the NMJ in *torsin* mutants were observed upon FISH of *discs-large* (*dlg*) RNA, which is not associated with nuclear DFz2C/LamC foci (Figures S4A–S4C) (Speese et al., 2012). Thus, in the absence of Torsin function, synaptic mRNAs known to be present in megaRNPs exhibit reduced localization at the NMJ, but a nonmegaRNP mRNA does not.

We also examined Par6 and MAGI protein levels using antibodies specific to *Drosophila* Par6 (Ruiz-Canada et al., 2004) and MAGI (this report). In wild-type larvae, Par6 and MAGI immunoreactivity localized primarily to the postsynaptic muscle region of the NMJ (Figures 4F and 4G, top panels). In addition, Par6 immunoreactivity was observed in a diffuse manner at presynaptic boutons (marked by the anti-HRP signal), being particularly prominent at presynaptic microtubule bundles (Ruiz-Canada et al., 2004) (Figure 4F, top panels) and at low levels at the muscle cell cortex (Figure 4F, top panels). MAGI immunoreactivity was also observed at presynaptic compartments, but without noticeable concentration at microtubule bundles (Figure 4G, top

Please cite this article in press as: Jokhi et al., Torsin Mediates Primary Envelopment of Large Ribonucleoprotein Granules at the Nuclear Envelope, Cell Reports (2013), http://dx.doi.org/10.1016/j.celrep.2013.03.015

Cell PRESS
Open ACCESS

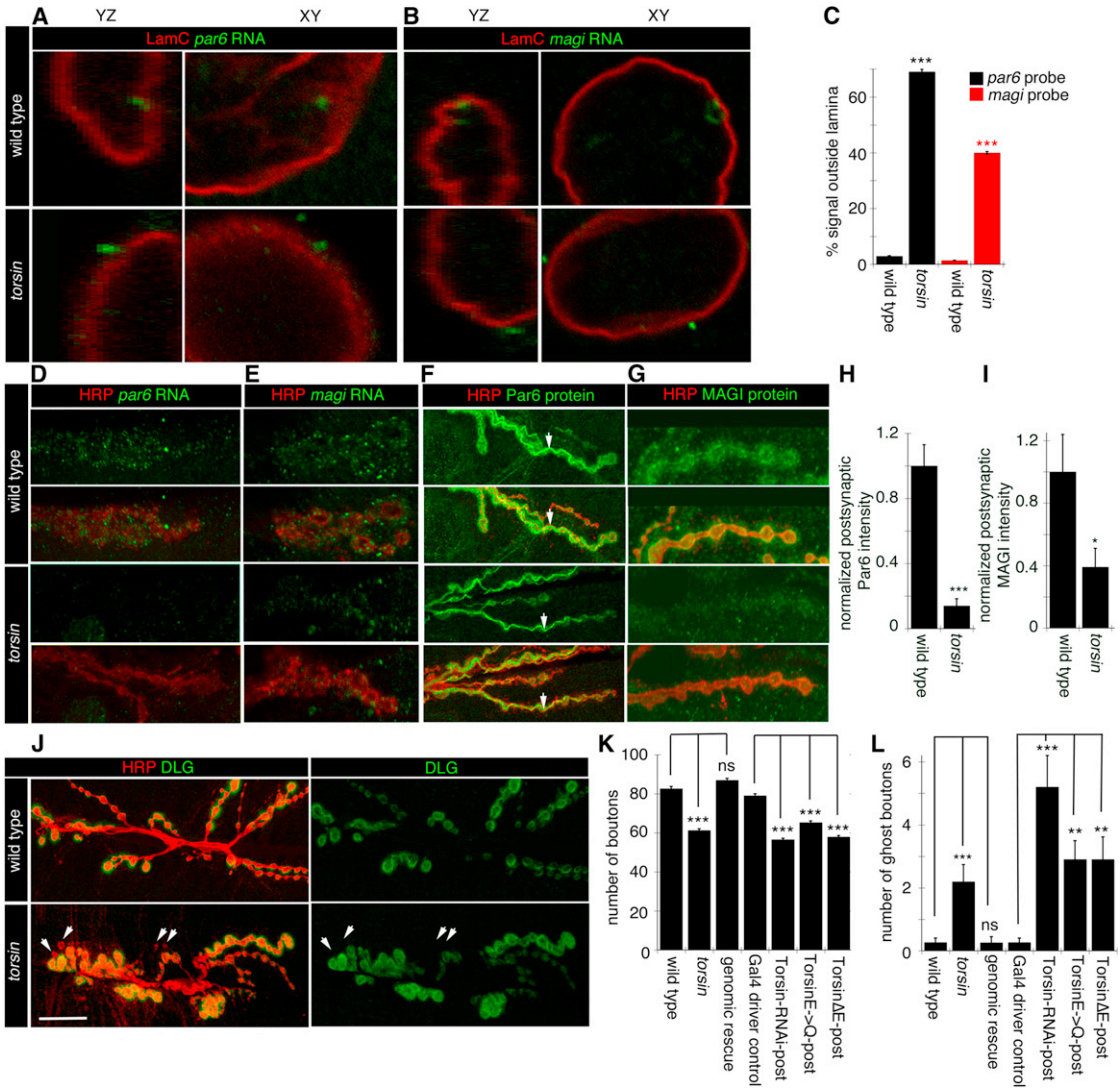

Figure 4. The Distribution of mRNAs at the NE and Synaptic Sites Is Disrupted in *torsin* Mutants

(A and B) FISH to body wall muscles showing the nuclear distribution of (A) *par6* and (B) *magi* transcripts in wild-type and *torsin* mutants.

(C) Quantification of FISH signal outside the nucleus. N [nuclei;larvae], [18;6],[18;6],[18;6],[14;6].

(D and E) FISH to body wall muscles showing the distribution of (D) *par6* and (E) *magi* transcript at the NMJ in wild-type and *torsin*-null mutants.

(F and G) Distribution of (F) Par6 and (G) Magi immunoreactivity at the NMJ in wild-type and *torsin* mutants.

(H and I) Quantification of postsynaptic (H) Par6 and (I) Magi immunoreactive signal, normalized to wild-type control. N([NMJs;larvae]) is [16;6],[18;6] (H) and [17;6],[15;6] (I).

(J) NMJs in wild-type and *torsin* mutants labeled with anti-HRP and anti-DLG showing reduced size and increased ghost boutons (arrowheads) in *torsin* mutants.

(K and L) Quantification of the number of (K) synaptic boutons and (L) ghost boutons. N([NMJs;larvae]), [19;10],[18;10],[19;10],[19;10],[20;10],[19;10],[19;10] for (K) and (L). Error bars represent ±SEM; **$p < 0.001$; ***$p < 0.0001$.

Calibration scale are 3 μm (A and B), 10 μm (D–G), and 20 μm (J). See also Figure S4.

panels). In *torsin*-null mutants, postsynaptic localization of Par6 immunoreactivity as well as muscle cell cortex signal was severely reduced (Figure 4F, bottom panels; Figure 4H), while presynaptic localization of Par6 at microtubule bundles appeared normal (Figure 4F, arrows). Similarly, postsynaptic MAGI protein localization was severely reduced in these mutants (Figure 4G, bottom panels; Figure 4I). Unlike Par6 and MAGI, DLG immunoreactivity was not changed in *torsin* mutants (Figure 4J; Figure S4D), suggesting that the defect is not general but affects only a subset of postsynaptic proteins. Thus, disrupting Torsin function prevents normal localization of some synaptic mRNAs and, as a consequence, normal postsynaptic levels of their encoded proteins.

The functional consequence on NMJ structure of reduced Par6 and MAGI mRNA and protein levels at the postsynaptic compartment in *torsin* mutants was assessed by counting the

number of normal and undifferentiated ghost boutons observable in the last (third-instar) larval stage. Interfering with Torsin function resulted in a significantly reduced number of synaptic boutons (Figures 4J and 4K) and a significantly increased number of undifferentiated ghost boutons (Figure 4J, arrowheads; Figure 4L).

Together, these results demonstrate that inhibiting Torsin function results in megaRNP accumulation at the NE, likely due to a defect in INM scission during primary envelopment. As a consequence, synaptic transcript-containing megaRNPs fail to efficiently exit the nucleus, limiting trafficking of the mRNAs contained within to postsynaptic sites where they are normally enriched. This reduced synaptic mRNA localization results in reduced levels of specific postsynaptic proteins during NMJ expansion and thus in poorly developed NMJs containing fewer synaptic boutons and increased numbers of undifferentiated ghost boutons lacking postsynaptic proteins. These results provide mechanistic insight into the molecular machinery underlying nuclear egress of megaRNPs by NE budding. They also provide a mechanism by which Torsin influences synaptic development as well as important clues as to how torsinA dysfunction might lead to the alterations in synaptic plasticity observed in DYT1 mouse models and human patients.

EXPERIMENTAL PROCEDURES

Fly Strains

Flies were reared on standard *Drosophila* medium at 25°C. RNAi crosses and controls were performed at 29°C.

Molecular Biology

Torsin dsRNA was prepared by amplifying exon1 by PCR and in vitro transcribed using the Ambion MEGAscript T7 kit.

S2 Cell Culture and dsRNA Treatment

Drosophila SL2-NP2 cells were cultured and treated as described in Koles et al. (2012).

Immunocytochemistry

Third-instar larval body wall muscles were dissected and fixed as described in Budnik et al. (1996).

Antibody Generation

Anti-MAGI was generated by immunizing rats with a bacterially produced Magi peptide (amino acids 337–558).

Fluorescence In Situ Hybridization

Procedures for FISH were as described in Speese et al. (2012)

Transmission Electron Microscopy

TEM was performed as described in Ashley et al. (2005).

Diaminobenzidine conversion of Mini-SOG

Diaminobenzidine (DAB) photoconversion was adapted from Grabham and Goldberg (1997).

Image Acquisition

Confocal images were acquired using a Zeiss LSM700 confocal microscope equipped with a Zeiss ×63 Plan-Apochromat 1.4 NA DIC oil-immersion objective.

Quantification

Categorization of DFz2C/LamC Foci at the Light Microscopy Level

For categorization of nuclear DFz2C/LamC foci, larval body wall muscle preparations were labeled with antibodies to DFz2C and LamC and the number of nuclei at muscle 6 (segments A2–A4) with foci of the following categories were counted and divided by the total number of nuclei. A focus was considered "normal" if it contained a DFz2C spot localized within a thickening of the lamina (Figure 1A), "with small DFz2C puncta" if small DFz2C puncta localized at the lamina but there was no observable thickening of the lamina at this site (Figure 1B), or "containing depleted foci" if a thickening of the lamina devoid of DFz2C signal was observed (Figure 1C).

Ultrastructural Categorization of megaRNPs

Micrographs of foci at 78,000–110,000X total magnification were examined and megaRNPs were categorized as "within INM invaginations" if they appeared as a granule or granule cluster surrounded by an INM invagination, as "with a collared neck" if the granule was located within an enlarged perinuclear space and tethered to the INM through an electron-dense neck, or as "amorphous" if the granule was larger than 250 nm.

Categorization of NE Associated FISH Signal

For determining the percentage of signal outside the lamina, the number of lamina-associated FISH puncta was subdivided into those that were present either on the nucleoplasmic or cytoplasmic side of the LamC-immunoreactive lamina.

Measurements of Postsynaptic Protein Levels

Normalized postsynaptic protein levels were determined as described in Ramachandran et al. (2009).

Quantification of Bouton and Ghost Bouton Number

Bouton and ghost bouton numbers were assessed as described in Speese et al. (2012).

Statistical Analysis

See Extended Experimental Procedures for complete statistical analysis.

SUPPLEMENTAL INFORMATION

Supplemental Information includes four figures and Extended Experimental Procedures and can be found with this article online at http://dx.doi.org/10.1016/j.celrep.2013.03.015.

LICENSING INFORMATION

This is an open-access article distributed under the terms of the Creative Commons Attribution License, which permits unrestricted use, distribution, and reproduction in any medium, provided the original author and source are credited.

ACKNOWLEDGMENTS

We thank Drs. Xandra Breakefield, Mary Munson, Reid Gilmore, Emiliano Ricci, and members of the Budnik lab for helpful comments on the manuscript and discussions. We would like to thank the University of Massachusetts Medical School Electron Microscopy Facility for support in our ultrastructural studies and the Vienna Drosophila RNAi facility for providing the Torsin-RNAi line. We also thank Drs. Pamela Gayer, Yosef Gruenbaum, Georg Krohne, and Gertrud Schupbach for the generous gift of antibodies. This work was supported by National Institutes of Health grant R01 NS063228 (to V.B.). M.J.M. is a Howard Hughes Medical Institute investigator. V.J. carried out most of the experiments and contributed intellectually to the project. J.A. carried out some of the ultrastructural studies and contributed intellectually to the project and manuscript writing. J.N. carried out most the ultrastructural experiments. A.N. performed supporting FISH in wild-type and mutant larvae. N.I. and N.W.-I. provided the unpublished Torsin$^{\Delta E}$ fly strain and contributed to discussions. M.J.M. provided critical intellectual input and helped write the manuscript. V.B. directed the project and wrote the manuscript.

Cell PRESS
Open ACCESS

Received: January 4, 2013
Revised: March 11, 2013
Accepted: March 12, 2013
Published: April 11, 2013

REFERENCES

Ashley, J., Packard, M., Ataman, B., and Budnik, V. (2005). Fasciclin II signals new synapse formation through amyloid precursor protein and the scaffolding protein dX11/Mint. J. Neurosci. *25*, 5943–5955.

Ataman, B., Ashley, J., Gorczyca, D., Gorczyca, M., Mathew, D., Wichmann, C., Sigrist, S.J., and Budnik, V. (2006). Nuclear trafficking of Drosophila Frizzled-2 during synapse development requires the PDZ protein dGRIP. Proc. Natl. Acad. Sci. USA *103*, 7841–7846.

Ataman, B., Ashley, J., Gorczyca, M., Ramachandran, P., Fouquet, W., Sigrist, S.J., and Budnik, V. (2008). Rapid activity-dependent modifications in synaptic structure and function require bidirectional Wnt signaling. Neuron *57*, 705–718.

Barco, A., Lopez de Armentia, M., and Alarcon, J.M. (2008). Synapse-specific stabilization of plasticity processes: the synaptic tagging and capture hypothesis revisited 10 years later. Neurosci. Biobehav. Rev. *32*, 831–851.

Breakefield, X.O., Blood, A.J., Li, Y., Hallett, M., Hanson, P.I., and Standaert, D.G. (2008). The pathophysiological basis of dystonias. Nat. Rev. Neurosci. *9*, 222–234.

Budnik, V., Koh, Y.H., Guan, B., Hartmann, B., Hough, C., Woods, D., and Gorczyca, M. (1996). Regulation of synapse structure and function by the Drosophila tumor suppressor gene dlg. Neuron *17*, 627–640.

Goodchild, R.E., Kim, C.E., and Dauer, W.T. (2005). Loss of the dystonia-associated protein torsinA selectively disrupts the neuronal nuclear envelope. Neuron *48*, 923–932.

Grabham, P.W., and Goldberg, D.J. (1997). Nerve growth factor stimulates the accumulation of beta1 integrin at the tips of filopodia in the growth cones of sympathetic neurons. J. Neurosci. *17*, 5455–5465.

Grünwald, D., Singer, R.H., and Rout, M. (2011). Nuclear export dynamics of RNA-protein complexes. Nature *475*, 333–341.

Iyer, L.M., Leipe, D.D., Koonin, E.V., and Aravind, L. (2004). Evolutionary history and higher order classification of AAA+ ATPases. J. Struct. Biol. *146*, 11–31.

Kim, C.E., Perez, A., Perkins, G., Ellisman, M.H., and Dauer, W.T. (2010). A molecular mechanism underlying the neural-specific defect in torsinA mutant mice. Proc. Natl. Acad. Sci. USA *107*, 9861–9866.

Köhler, A., and Hurt, E. (2007). Exporting RNA from the nucleus to the cytoplasm. Nat. Rev. Mol. Cell Biol. *8*, 761–773.

Koles, K., Nunnari, J., Korkut, C., Barria, R., Brewer, C., Li, Y., Leszyk, J., Zhang, B., and Budnik, V. (2012). Mechanism of evenness interrupted (Evi)-exosome release at synaptic boutons. J. Biol. Chem. *287*, 16820–16834.

Maric, M., Shao, J., Ryan, R.J., Wong, C.S., Gonzalez-Alegre, P., and Roller, R.J. (2011). A functional role for TorsinA in herpes simplex virus 1 nuclear egress. J. Virol. *85*, 9667–9679.

Mathew, D., Ataman, B., Chen, J., Zhang, Y., Cumberledge, S., and Budnik, V. (2005). Wingless signaling at synapses is through cleavage and nuclear import of receptor DFrizzled2. Science *310*, 1344–1347.

Mettenleiter, T.C., Klupp, B.G., and Granzow, H. (2006). Herpesvirus assembly: a tale of two membranes. Curr. Opin. Microbiol. *9*, 423–429.

Naismith, T.V., Heuser, J.E., Breakefield, X.O., and Hanson, P.I. (2004). TorsinA in the nuclear envelope. Proc. Natl. Acad. Sci. USA *101*, 7612–7617.

Neuwald, A.F., Aravind, L., Spouge, J.L., and Koonin, E.V. (1999). AAA+: A class of chaperone-like ATPases associated with the assembly, operation, and disassembly of protein complexes. Genome Res. *9*, 27–43.

Ozelius, L.J., Hewett, J.W., Page, C.E., Bressman, S.B., Kramer, P.L., Shalish, C., de Leon, D., Brin, M.F., Raymond, D., Corey, D.P., et al. (1997). The early-onset torsion dystonia gene (DYT1) encodes an ATP-binding protein. Nat. Genet. *17*, 40–48.

Packard, M., Koo, E.S., Gorczyca, M., Sharpe, J., Cumberledge, S., and Budnik, V. (2002). The Drosophila Wnt, wingless, provides an essential signal for pre- and postsynaptic differentiation. Cell *111*, 319–330.

Ramachandran, P., Barria, R., Ashley, J., and Budnik, V. (2009). A critical step for postsynaptic F-actin organization: regulation of Baz/Par-3 localization by aPKC and PTEN. Dev. Neurobiol. *69*, 583–602.

Richter, J.D. (2001). Think globally, translate locally: what mitotic spindles and neuronal synapses have in common. Proc. Natl. Acad. Sci. USA *98*, 7069–7071.

Ruiz-Canada, C., Ashley, J., Moeckel-Cole, S., Drier, E., Yin, J., and Budnik, V. (2004). New synaptic bouton formation is disrupted by misregulation of microtubule stability in aPKC mutants. Neuron *42*, 567–580.

Shu, X., Lev-Ram, V., Deerinck, T.J., Qi, Y., Ramko, E.B., Davidson, M.W., Jin, Y., Ellisman, M.H., and Tsien, R.Y. (2011). A genetically encoded tag for correlated light and electron microscopy of intact cells, tissues, and organisms. PLoS Biol. *9*, e1001041.

Speese, S.D., Ashley, J., Jokhi, V., Nunnari, J., Barria, R., Li, Y., Ataman, B., Koon, A., Chang, Y.-T., Li, Q., et al. (2012). Nuclear envelope budding enables large ribonucleoprotein particle export during synaptic Wnt signaling. Cell *149*, 832–846.

Tanabe, L.M., Kim, C.E., Alagem, N., and Dauer, W.T. (2009). Primary dystonia: molecules and mechanisms. Nat. Rev. Neurol. *5*, 598–609.

Wakabayashi-Ito, N., Doherty, O.M., Moriyama, H., Breakefield, X.O., Gusella, J.F., O'Donnell, J.M., and Ito, N. (2011). Dtorsin, the Drosophila ortholog of the early-onset dystonia TOR1A (DYT1), plays a novel role in dopamine metabolism. PLoS ONE *6*, e26183.

Walker, J.E., Saraste, M., Runswick, M.J., and Gay, N.J. (1982). Distantly related sequences in the alpha- and beta-subunits of ATP synthase, myosin, kinases and other ATP-requiring enzymes and a common nucleotide binding fold. EMBO J. *1*, 945–951.

Wiersma-Meems, R., Van Minnen, J., and Syed, N.I. (2005). Synapse formation and plasticity: the roles of local protein synthesis. Neuroscientist *11*, 228–237.